

Signatures of accretion events in the halos of early-type galaxies from comparing PNe and GCs kinematics

L. Coccato^{1*}, O. Gerhard², M. Arnaboldi^{1,3}

¹European Southern Observatory, Karl-Schwarzschild-Straße 2, 85748 Garching bei München, Germany.

²Max-Planck-Institut für extraterrestrische Physik, Postfach 1312, Giessenbachstr., D-85741 Garching bei München, Germany.

³INAF, Osservatorio Astronomico di Pino Torinese, I-10025 Pino Torinese, Italy.

received: 05 July 2012; accepted: yyy

ABSTRACT

We have compared the halo kinematics traced by globular clusters (GCs) and planetary nebulae (PNe) for two elliptical galaxies in dense environments (NGC 1399 and NGC 4649) and for the merger remnant Cen A. We find differences in the rotational properties of the PNe, red GCs, or blue GCs systems in all three galaxies and some indication for substructures. We interpret these as signatures of tidal stripping or accretion of small galaxies, showing that low luminosity and dwarf galaxies have a higher specific frequency of GCs than PNe.

Key words: galaxies: elliptical and lenticular, cD; galaxies: haloes; galaxies: individual: NGC 1399, NGC 4649, NGC 5128; galaxies: kinematics and dynamics.

1 INTRODUCTION

Stellar halos of galaxies offer an important laboratory to understand the galaxies’ formation process and evolution. The dynamic time scales in the halos are large, and the imprint of the formation mechanisms may still be preserved at large radii in the kinematics, in the orbital structure, in streams and substructures, or in the chemical composition and distribution of stars.

Due to the rapid dimming of the stellar light at large radii, alternate tracers of the underlying stellar population are studied. Planetary Nebulae (PNe) and Globular Clusters (GCs) can be detected in large numbers out to several effective radii, and have been used to probe the kinematics (e.g. Coccato et al. 2009; Herrmann & Ciardullo 2009; Teodorescu et al. 2010; Lee et al. 2010; Schuberth et al. 2012), dark matter content (e.g. Côté et al. 2001; Romanowsky et al. 2003; de Lorenzi et al. 2009; Napolitano et al. 2011; Richtler et al. 2011; Deason et al. 2012) and chemical composition (e.g. Forbes et al. 2011; Alves-Brito et al. 2011) of the stellar halos in nearby galaxies. PNe have been found to be a good tracers of the underlying stellar population, as their spatial distribution and kinematics well agree with those of the stars (Coccato et al. 2009). This is still not so clear for GCs: they have a bimodal color distribution (see the review by Brodie & Strader 2006 and references therein) where red GCs (metal rich) have a radial density distribution similar to that of the stars and PNe, while blue GCs (metal poor) have a more extended distribution.

Recently, the distribution and kinematics of PNe and GCs in galaxy halos have been exploited also to detect substructures, which are interpreted as signatures of minor mergers and accre-

tion events that contribute to the build up of the stellar halos in early-type galaxies (Shih & Méndez 2010; Woodley & Harris 2011; Romanowsky et al. 2012) or to the disk heating in spirals (Herrmann et al. 2009b).

So far, a direct and detailed comparison between the two-dimensional velocity fields inferred by GCs or PNe has been done only in few cases. The commonly used approach was either to combine the two datasets in the analysis, or use the most suited dataset to study a particular science case. Little attention was put in the information potentially contained in the “discrepancies” between the PNe and GCs velocity fields. We therefore compared the halo kinematics independently traced by GCs and PNe in a sample of galaxies. In this paper, we describe the properties of 3 galaxies in our sample (namely NGC 1399, NGC 4649 and NGC 5128), whose two-dimensional velocity fields have kinematic quantities that are different for PNe and GCs. The complete analysis of the entire sample will be presented in a forthcoming paper. Here we concentrate on the average kinematic properties and we do not discuss the radial distribution of individual tracers.

2 HALO KINEMATICS

We reconstruct the mean two-dimensional velocity fields $\langle V \rangle$ for the PNe, red-GCs and blue-GCs systems using an adaptive Gaussian kernel smoothing technique, which was defined and tested in Coccato et al. (2009). 3σ velocity outliers are iteratively removed through the *friendless* algorithm as in Merrett et al. (2006). We do not assume any particular symmetry of the data to not bias the analysis towards any preferential configuration or symmetry. The PNe and GCs detected in NGC 1399 and NGC 4649 contain objects associated to the companion galaxies (NGC 1404

* E-mail: lcoccato@eso.org

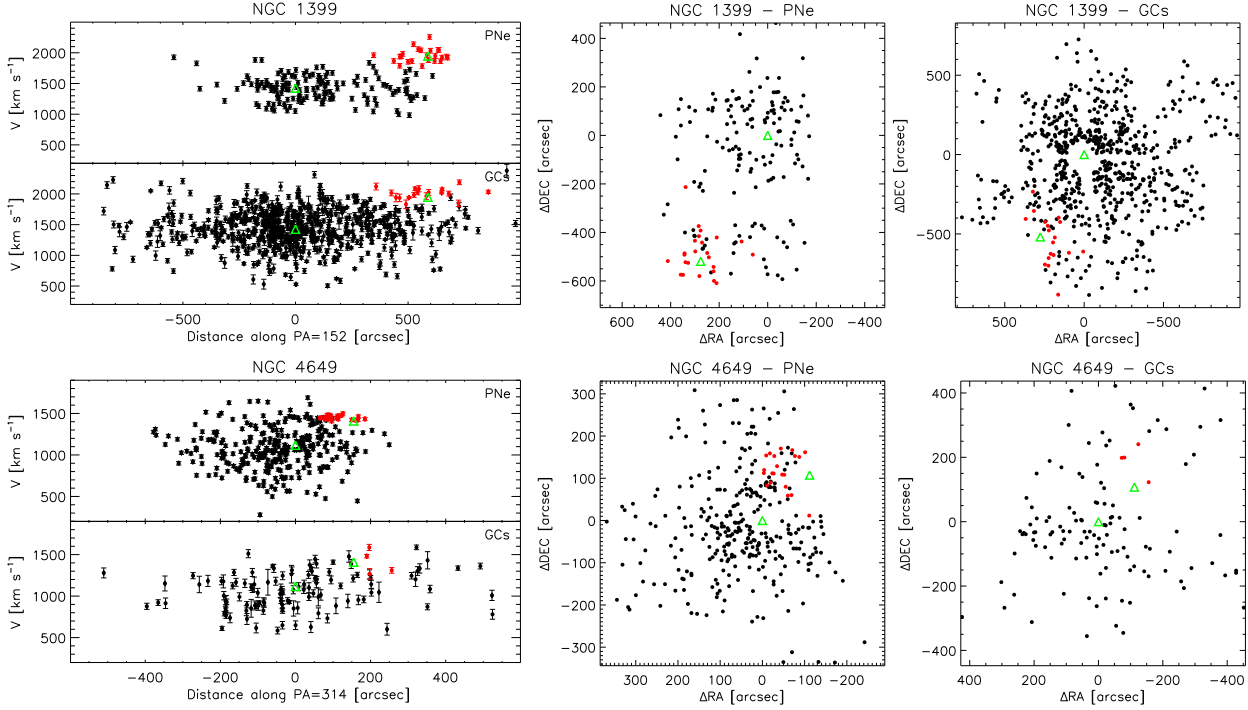


Figure 1. Membership allocation of PNe and GCs between the main galaxies (NGC 1399 and NGC 4697) and their companion (NGC 1404 and NGC 4647). The first figure in each row shows the radial velocity of PNe and GCs as a function of their position along the line connecting the main galaxy to the companion. The second and third figures in each row show the location of the PNe and GCs on the sky. Objects marked with red have more than 60% probability to belong to the companion galaxy, and therefore are removed from the analysis. Green triangles mark the position of the galaxies and the companions.

and NGC 4647, respectively). Therefore, we have to remove the contaminants before recovering the velocity fields.

To do that, we use the procedure described in McNeil et al. (2010), which assigns to each object (PNe or GCs) a probability to belong to the galaxy or to the companion on the basis of the galaxies' surface brightnesses at the objects' positions and of the line of sight velocity distributions. We removed from the analysis all objects that have more than 60% of probability to belong to the companion galaxy (see Figure 1). This is different from what was typically used as criterion in the past (e.g. objects with more than 95% probability to belong to the main galaxy were kept) because we want to include in the analysis also those objects that may have been stripped from the companion and thus trace an on-going interaction. The reconstructed mean two-dimensional velocity fields of PNe, red and blue GCs are shown in Figure 2.

We measure the amount and direction of rotation as a function of radius for each of the components (PNe, red and blue GCs) in each galaxy by fitting the following function for several radial bins:

$$\langle V \rangle (\phi; R) = V_{\text{sys}}(R) + V_{\text{rot}}(R) \cdot \cos[\phi - PA_{\text{kin}}(R)] \quad (1)$$

R is the distance of the object (PNe or GCs) from the galaxy center, ϕ is its position angle on the sky, $\langle V \rangle$ is the mean velocity of the objects at a given position on the sky. The fit variables for each radial bin are: V_{rot} (amplitude of rotation), V_{sys} (mean velocity), and PA_{kin} (kinematic position angle). V_{sys} is found to be consistent with the galaxy systemic velocity at all radii. Angles are measured from North towards East. Errors on the measured fit variables V_{sys} , V_{rot} , and PA_{kin} , are computed by means of Monte Carlo simulations. We create 500 mock catalogs with simulated velocities $V_{\text{LOS}}^{\text{sim}}$ for each object drawn from a Gaussian distribution with mean V_{LOS} and standard deviation that includes the lo-

cal velocity dispersion and measurement errors. We then reprocess the simulated catalogs and get 500 simulated fit parameters, whose standard deviations define the errors of our fit variables.

In the following, we describe the results obtained for the 3 galaxies individually.

NGC 1399. PNe data are from McNeil et al. (2010), GCs data are from Schuberth et al. (2010).

The PNe system is dominated by random motions ($\langle \sigma \rangle \sim 220 \text{ km s}^{-1}$), but it shows also small rotation along two opposite directions. Innermost $R < 200''$ PNe rotate slowly ($V_{\text{rot}} = 31 \pm 20 \text{ km s}^{-1}$) along $PA_{\text{kin}} = 231^\circ \pm 50^\circ$, consistent with the galaxy photometric major axis ($PA = 290^\circ$, Dirsch et al. 2003). On the contrary, outermost $R > 300''$ PNe rotate slightly faster ($V_{\text{rot}} = 47 \pm 27 \text{ km s}^{-1}$) and along a nearly opposite direction ($PA_{\text{kin}} = 46^\circ \pm 47^\circ$). The PNe two-dimensional velocity field is in agreement with that shown in McNeil et al. (2010).

We divide the GCs in NGC 1399 in red and blue GCs as in Schuberth et al. (2010). They find a rotation of $V = 110 \pm 53 \text{ km s}^{-1}$ for the outermost ($4' < R \leq 8'$) blue-GCs. From Equation 1, we find consistent values in the same radial range ($V_{\text{rot}} = 79 \pm 29 \text{ km s}^{-1}$). Nevertheless, by looking at Fig. 2, both the red and blue GCs do not display a well defined direction of rotation: their mean velocity fields are rather characterized by substructures. The two more evident are located on the South and North East sides of NGC 1399. In Figure 3 we show the line of sight velocity distributions in these regions. In the S substructure, the PNe and GCs have median velocities that differ at $\sim 1.2\sigma$ level. From a Kolmogorov-Smirnov test (Press et al. 2002), the probability that PNe and red (blue) GCs are drawn from the same distribution is $1 \pm 1\%$ ($8 \pm 5\%$); this probability is higher when comparing the red and blue GCs distributions ($69 \pm 22\%$). In the NE substructure,

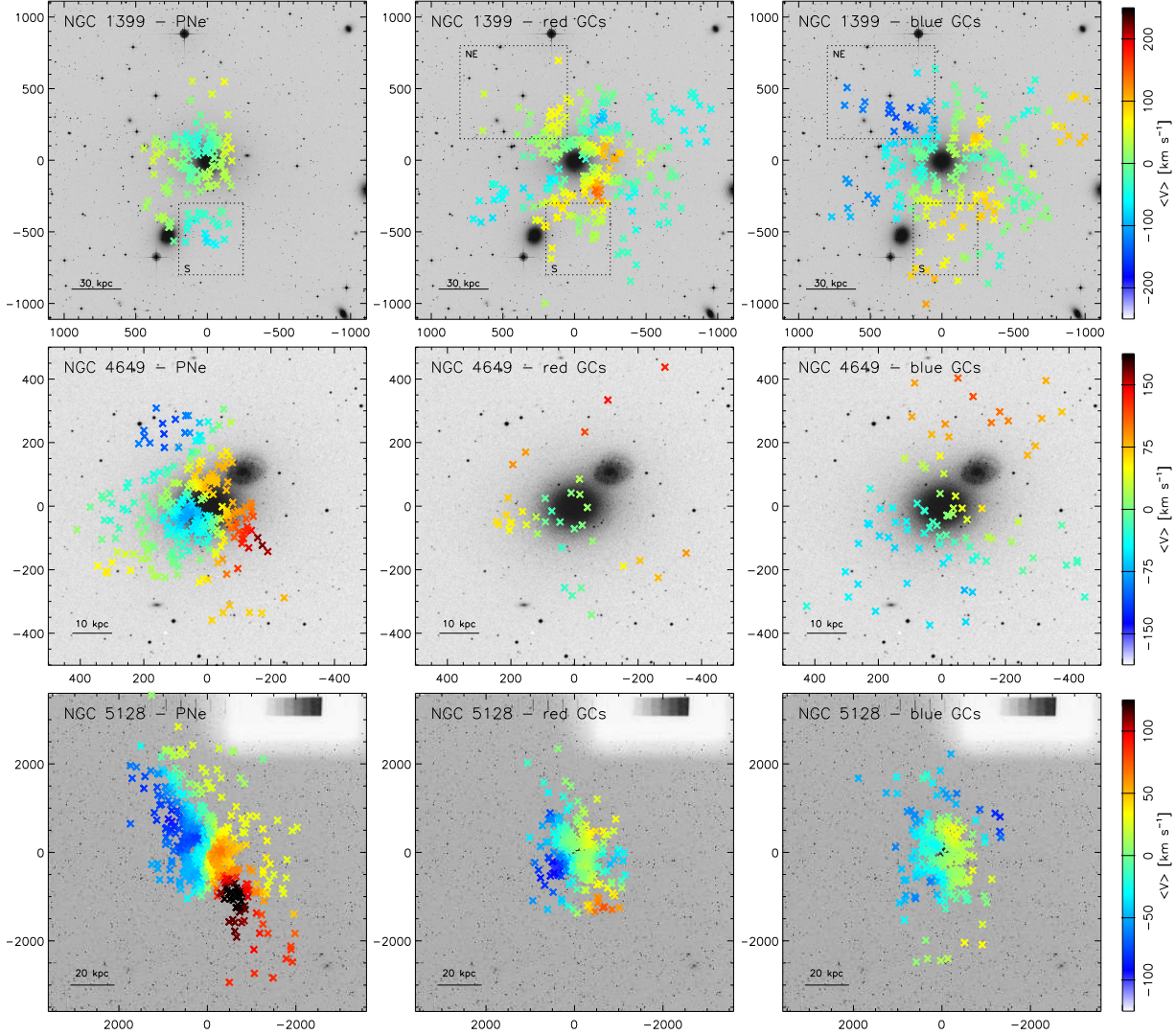


Figure 2. Mean velocity fields for NGC 1399 (top panels), NGC 4649 (middle panels) and NGC 5128 (bottom panels). Each panel shows the galaxy image, where the positions of the PNe and GCs are marked with crosses. The colors indicate the values of the mean velocity field computed at that position. North is up, East is left. Coordinates are in arcseconds. The dashed lines define regions where kinematic substructures in NGC 1399 are identified (see text for details).

ture, the median velocities of red and blue GCs differ at $\sim 1.2\sigma$ level (no PNe are detected in this region), and the probability that they are drawn from the same distribution is $3 \pm 2\%$. Note that Fig. 3 shows V_{LOS} , which are independent of the kernel smoothing technique used to recover the mean velocity fields.

NGC 4649. PNe data are from Teodorescu et al. (2011), GCs data are from Lee et al. (2008).

The PNe system is dominated by dispersion ($\langle \sigma \rangle \sim 250 \text{ km s}^{-1}$) and it shows two main kinematic substructures. PNe in the inner $R < 60''$ rotate with an amplitude $V_{\text{rot}} = 77 \pm 22 \text{ km s}^{-1}$ along $PA_{\text{kin}} = 302^\circ \pm 20^\circ$, consistent with the photometric major axis ($PA = 285^\circ$, de Vaucouleurs et al. 1991). PNe in the outer $R > 250''$ rotate around an orthogonal direction ($PA_{\text{kin}} = 205^\circ \pm 18^\circ$) with the same amplitude ($V_{\text{rot}} = 75 \pm 29 \text{ km s}^{-1}$). The two-dimensional velocity field is similar to that shown by Das et al. (2011), obtained using different criteria for contaminants removal.

We divide the GCs system of NGC 4649 in red and blue GCs as in Lee et al. (2008). The velocity field of the red GCs is not easily described by Eqn. 1, therefore it is not possible to define an ampli-

tude and direction of rotation. The blue GCs system shows a more regular velocity field. In the inner $R < 60''$ the blue GCs rotate along $PA_{\text{kin}} = 292^\circ \pm 31^\circ$ with an amplitude of $V_{\text{rot}} = 33 \pm 17 \text{ km s}^{-1}$, slower than the PNe in the same radial range but along similar direction. The PA_{kin} and V_{rot} increase gradually with the radius. At $R > 300''$ we measure rotation $V_{\text{rot}} = 82 \pm 20 \text{ km s}^{-1}$ along $PA_{\text{kin}} = 342^\circ \pm 88^\circ$, nearly opposite to that of the outermost PNe.

The stars in NGC 4649 within $\sim 25''$ rotate along a direction very similar to those of the inner PNe and blue GCs ($PA_* = 271.5^\circ \pm 3.8^\circ$) with an amplitude of $\sim 94 \text{ km s}^{-1}$ (Krajnović et al. 2011). The stellar rotation agrees with that of PNe, but it is larger than that of the blue GCs. This difference is probably due to the spatial incompleteness in the center that overestimates the kernel amplitude adopted in this region, causing a dilution effect when computing the local mean velocity field.

The dependence on radius of V_{rot} and PA_{kin} for stars, PNe, and blue GCs in NGC 4649 are shown in Figure 4.

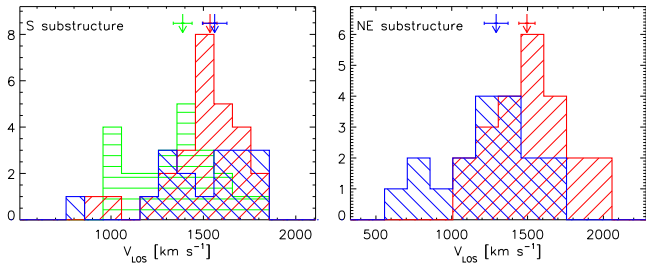


Figure 3. Velocity distribution of PNe (green), red GCs (red) and blue GCs (blue) in the South (left panel) and North East (right panel) substructures of NGC 1399. Arrows mark the median radial velocities of the systems with the same colors. Velocities are in the heliocentric reference system.

NGC 5128. PNe data are from Peng et al. (2004a), GCs data are from Woodley et al. (2010a,b).

The PNe and GCs kinematics in NGC 5128 were previously compared by (Peng et al. 2004b) and Woodley et al. (2007, 2010b). Here, we re-analyze these data sets uniformly with respect to those of the other galaxies in our sample, finding consistent results with their studies. Following Woodley et al. (2010b), we use the GCs metallicity $[\text{Fe}/\text{H}] = -1$ as threshold to separate red (metal rich) and blue (metal poor) GCs.

The PNe velocity field shows disk-like rotation, with a twist in the central 5 kpc due to the triaxiality of the system (see also Peng et al. 2004a). The small asymmetry between the directions of the approaching and receding side of the galaxy are probably due to the non uniform sampling of PNe in the outer regions. From Eq. 1 we find that PNe reach a maximum rotation $V_{\text{rot}} = 87 \pm 13 \text{ km s}^{-1}$ around $20'$, and then a decline to $V_{\text{rot}} = 56 \pm 13 \text{ km s}^{-1}$ in the halo (consistent with Woodley et al. 2007). The velocity dispersion is $\sim 140 \text{ km s}^{-1}$ in the center and then it declines with radius down to $\sim 80 \text{ km s}^{-1}$.

GCs do not show a clear disk-like rotation as PNe, especially the blue GCs. Central velocity dispersion of GCs is consistent with that of PNe, but it does not decline with radius. This support a picture where the GCs are more related to a spheroidal component, while the PNe are more related to a disk-like component.

3 DISCUSSION AND CONCLUSIONS

We showed in Sect. 2 that the PNe and GCs systems in NGC 1399, NGC 4649 and NGC 5128 have different kinematic properties. NGC 1399 and NGC 4649 are located in dense environments and have a luminous companion, respectively NGC 1404 and NGC 4647, while NGC 5128 is considered a merger remnant (e.g. Peng et al. 2004b; Woodley et al. 2010a and references therein). Therefore, the observed discrepancy between PNe and GCs kinematics in these galaxies could be related to the environment or to the merging history. We now discuss some scenarios:

Tidal stripping. NGC 1399 and NGC 4649 could have stripped material from their less massive companions. The GCs system (the blue GCs in particular) is generally more extended than the underlying stellar population (e.g. Harris 1991); this implies that in some cases only the outer GCs will be stripped by the tidal interaction, and no stars and PNe. If this is the case, the signature of the tidal stripping will be visible preferentially in the blue GCs system, which will therefore trace different kinematics than the PNe and stars. Forbes et al. (1997) explored this scenario for NGC 1399. This galaxy has an high specific frequency

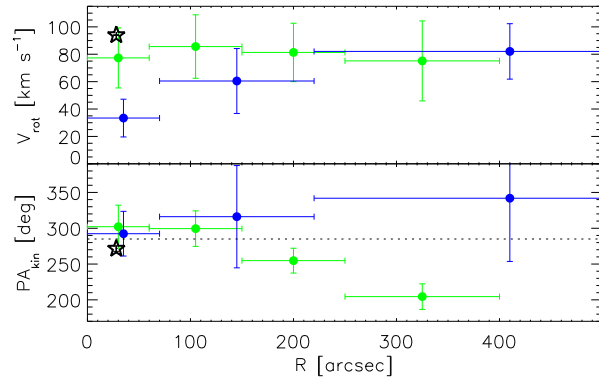


Figure 4. Rotation amplitude (V_{rot}) and direction (PA_{kin}) of the stars (black star), PNe (green), and blue GCs (blue) systems in NGC 4649, as obtained from Equation 1. The dotted lines indicate the photometric major axis position angle.

(i.e. number of GCs per unit galaxy luminosity, normalized at $M_V = 15$, Harris & van den Bergh 1981), and GCs are preferentially distributed in the outer galaxy regions. This suggests that some GCs in NGC 1399 may come from NGC 1404, which has a low specific frequency, consistent with having lost many of its GCs. Moreover, NGC 1404 has an observed luminosity which is consistent with its stellar velocity dispersion, suggesting that only a small fraction of its stars were removed in the stripping process.

Within the GCs system, the hypothesis that blue GCs can trace the interaction between the two galaxies more clearly than the red GCs system is supported by the following considerations: i) the majority of GCs with redshifted velocities in NGC 4649 are blue, and are located on the NGC 4647 side (Figs. 1 and 2); and ii) the blue GCs in the South substructure of NGC 1399 (close to its companion) have a broader line of sight velocity distribution than the red GCs in the same region.

Kinematic disturbances from a companion. Kinematic disturbances induced by the gravitational interaction with the companion can generate asymmetries in the stellar and ionized-gas velocity fields as observed in interacting binary galaxies (e.g. Borne et al. 1994) and galaxies in clusters (e.g. Rubin et al. 1999). However, stars, PNe and GCs would feel the same gravitational influence from the companion, and therefore they would trace the same velocity fields. Thus, we exclude this scenario.

Multiple mergers and accretion episodes. Massive galaxies in dense environments are subject to many merger and accretion events of different kinds (e.g. De Lucia & Blaizot 2007). Although NGC 5128 does not live in an environment as dense as those of NGC 1399 and NGC 4649, the presence of substructures (Woodley & Harris 2011; Mouhcine et al. 2011) suggests that NGC 5128 experienced significant accretion episodes in the past, perhaps from late infall of tidal tail material after the merger. If the fractions of accreted GCs and stars/PNe differ, the kinematic signature would be more visible in one system than in the other. It is therefore interesting to compare the expected number of accreted GCs and PNe for various galaxies to see whether there is a particular class of galaxies that would leave a kinematic signature preferentially in GCs or PNe. In Figure 5 we compare the expected number of accreted GCs and PNe as a function of the total magnitude and morphological type of the accreted galaxy. Despite of the scatter, the low statistics for dwarf galaxies, and the different observational constraints for PNe and GCs, there is indication that low luminosity and dwarf galaxies contribute more GCs than PNe. On

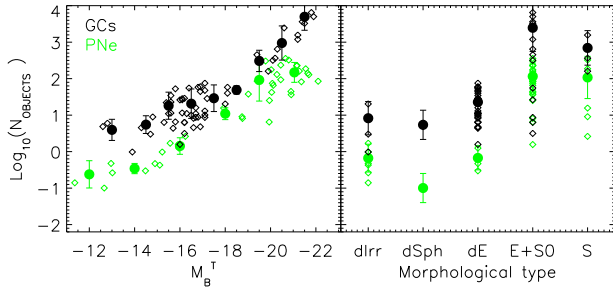


Figure 5. Expected number of sources (GCS or PNe) as a function of galaxy absolute magnitude (left) and morphology (right). GCS data are from Brodie & Strader (2006) and references therein. PNe data are from Zijlstra et al. (2006), Buzzoni et al. (2006), Coccato et al. (2009), and references therein. The expected number of GCs and PNe are computed from i) the specific frequencies, S_N (Harris & van den Bergh 1981) and $\alpha_{1,B}$ (Jacoby 1980), for GCs and PNe respectively, and ii) the total luminosities in the V and B bands, for GCs and PNe respectively.

the contrary, the expected contributions from bright spiral galaxies are more similar. Therefore, when a massive galaxy accretes many low luminosity galaxies and dwarfs, it will preferentially accrete GCs. Thus, the signature of the merging events will be imprinted in the GCs kinematics system more strongly, and differences in the velocity fields of GCs and PNe are to be expected.

To summarize, there is good indication that the velocity fields of PNe and GCs are different; to explore this better will require large homogeneous samples of both tracers. Such differences can be interpreted as a signature of accretion of dwarf galaxies or tidal stripping of GCs, which are more loosely bound than PNe. It would be interesting to compare the PNe and GCs kinematics in other massive galaxies in dense environments, like NGC 4889 (Coccato et al. 2010a,b), NGC 3311 (Coccato et al. 2011; Arnaboldi et al. 2012), M87 (Romanowsky et al. 2012), and NGC 1316 (Richtler et al. 2012), where the evidence for accretion of smaller galaxies comes from independent arguments and techniques.

ACKNOWLEDGMENTS

LC is supported by the European Community's Seventh Framework Programme (FP7/2007-2013/) under grant agreement No 229517. We thank K. Woodley and E. McNeil-Moylan for providing updated datasets for NGC 5128 and NGC 1399, and M. Lucio for useful discussion.

REFERENCES

Alves-Brito A., Hau G. K. T., Forbes D. A., et al. 2011, *MNRAS*, 417, 1823
 Arnaboldi M., Ventimiglia G., Iodice E., et al. 2012, *ArXiv*: 1205.5289
 Borne K. D., Balcells M., Hoessel J. G., et al. 1994, *ApJ*, 435, 79
 Brodie J. P., Strader J., 2006, *ARA&A*, 44, 193
 Buzzoni A., Arnaboldi M., Corradi R. L. M., 2006, *MNRAS*, 368, 877
 Coccato L., Arnaboldi M., Gerhard O., et al. 2010a, *A&A*, 519, 95
 Coccato L., Gerhard O., Arnaboldi M., 2010b, *MNRAS*, 407, L26

Coccato L., Gerhard O., Arnaboldi M., et al. 2009, *MNRAS*, 394, 1249
 Coccato L., Gerhard O., Arnaboldi M., et al. 2011, *A&A*, 533, 138
 Côté P., McLaughlin D. E., Hanes D. A., et al. 2001, *ApJ*, 559, 828
 Das P., Gerhard O., Mendez R. H., et al. 2011, *MNRAS*, 415, 1244
 de Lorenzi F., Gerhard O., Coccato L., et al. 2009, *MNRAS*, 395, 76
 De Lucia G., Blaizot J., 2007, *MNRAS*, 375, 2
 de Vaucouleurs G., de Vaucouleurs A., Corwin Jr. H. G., et al. 1991, *Third Reference Catalogue of Bright Galaxies (RC3)*
 Deason A. J., Belokurov V., Evans N. W., et al. 2012, *ApJ*, 748, 2
 Dirsch B., Richtler T., Geisler D., et al. 2003, *AJ*, 125, 1908
 Forbes D. A., Brodie J. P., Grillmair C. J., 1997, *AJ*, 113, 1652
 Forbes D. A., Spitler L. R., Strader J., et al. 2011, *MNRAS*, 413, 2943
 Harris W. E., 1991, *ARA&A*, 29, 543
 Harris W. E., van den Bergh S., 1981, *AJ*, 86, 1627
 Herrmann K. A., Ciardullo R., 2009, *ApJ*, 705, 1686
 Herrmann K. A., Ciardullo R., Sigurdsson S., 2009b, *ApJ*, 693, L19
 Jacoby G. H., 1980, *ApJS*, 42, 1
 Krajnović D., Emsellem E., Cappellari M., et al. 2011, *MNRAS*, 414, 2923
 Lee M. G., Hwang H. S., Park H. S., et al. 2008, *ApJ*, 674, 857
 Lee M. G., Park H. S., Hwang H. S., et al. 2010, *ApJ*, 709, 1083
 McNeil E. K., Arnaboldi M., Freeman K. C., et al. 2010, *A&A*, 518, A44
 Merrett H. R., Merrifield M. R., Douglas N. G., Kuijken K., Romanowsky A. J., et al. 2006, *MNRAS*, 369, 120
 Mouhcine M., Ibata R., Rejkuba M., 2011, *MNRAS*, 415, 993
 Napolitano N. R., Romanowsky A. J., Capaccioli M., et al. 2011, *MNRAS*, 411, 2035
 Peng E. W., Ford H. C., Freeman K. C., 2004a, *ApJ*, 602, 685
 Peng E. W., Ford H. C., Freeman K. C., 2004b, *ApJ*, 602, 705
 Press W. H., Teukolsky S. A., Vetterling W. T., et al. 2002, *Numerical recipes in C++ : the art of scientific computing*
 Richtler T., Bassino L. P., Dirsch B., et al. 2012, *A&A (ArXiv)*: 1203.1879
 Richtler T., Salinas R., Misgeld I., et al. 2011, *A&A*, 531, A119
 Romanowsky A. J., Douglas N. G., Arnaboldi M., et al. 2003, *Science*, 301, 1696
 Romanowsky A. J., Strader J., Brodie J. P., et al. 2012, *ApJ*, 748, 29
 Rubin V. C., Waterman A. H., Kenney J. D. P., 1999, *AJ*, 118, 236
 Schuberth Y., Richtler T., Hilker M., et al. 2010, *A&A*, 513, A52
 Schuberth Y., Richtler T., Hilker M., et al. 2012, *ArXiv*: 1205.2093
 Shih H.-Y., Méndez R. H., 2010, *ApJ*, 725, L97
 Teodorescu A. M., Méndez R. H., Bernardi F., Riffeser A., Kudritzki R. P., 2010, *ApJ*, 721, 369
 Teodorescu A. M., Méndez R. H., Bernardi F., Thomas J., Das P., Gerhard O., 2011, *ApJ*, 736, 65
 Woodley K. A., Gómez M., Harris W. E., et al. 2010b, *AJ*, 139, 1871
 Woodley K. A., Harris W. E., 2011, *AJ*, 141, 27
 Woodley K. A., Harris W. E., Beasley M. A., et al. 2007, *AJ*, 134, 494
 Woodley K. A., Harris W. E., Puzia T. H., et al. 2010a, *ApJ*, 708, 1335

Zijlstra A. A., Matsuura M., Wood P. R., et al. 2006, MNRAS, 370, 1961